Coppola R.E. (Orcid ID: 0000-0001-7913-7007)

Synthesis, characterization and performance of new DABCO derivatives in anion exchange membranes

R.E. Coppola[a], N.B. D'Accorso[b, c], G.C. Abuin[d]

[a]Instituto Nacional de Tecnología Industrial (INTI), Departamento de Nanomateriales Funcionales, Micro y Nanotecnologías, Av. General Paz 5445, San Martín B1650KNA, Buenos Aires, Argentina

[b]Universidad de Buenos Aires, Facultad de Ciencias Exactas y Naturales, Departamento de Química Orgánica, Buenos Aires, Argentina

[c]CONICET- Universidad de Buenos Aires, Centro de Investigaciones en Hidratos de Carbono (CIHIDECAR), Buenos Aires, Argentina

[d]Instituto Nacional de Tecnología Industrial (INTI), Departamento de Almacenamiento y Conversión de la Energía, Av. General Paz 5445, B1650KNA, San Martín, Buenos Aires, Argentina.

Corresponding author: rcoppola@inti.gob.ar

Abstract:

Anion exchange membranes have aroused much interest for used in electrolyzers and alkaline fuel cells. In this work, two double charged anion exchange membranes based on poly(2,5-benzimidazole) (ABPBI) and poly(vinylbenzyl chloride) (PVBC) prepared by the casting method are reported. The effect of two different quaternizing agents based in 1,4-diazabicyclo[2.2.2]octane (DABCO) was evaluated. These membranes were characterized by means of Fourier transform infrared spectroscopy, scanning electron microscopy, thermal gravimetric analysis, water contact angle, swelling ratio, KOH and water uptake, ionic exchange capacity and ionic conductivity. Results showed that the length of the alkyl chain has a strong effect in the membrane properties. A good performance in a zero-gap water alkaline electrolyzer was obtained for the membrane based in the butyl derivate of DABCO (BDABCO).

Keywords: Anion exchange membrane; polybenzimidazole; crosslinked; DABCO head group; electrolyzer.

This article has been accepted for publication and undergone full peer review but has not been through the copyediting, typesetting, pagination and proofreading process which may lead to differences between this version and the Version of Record. Please cite this article as doi: 10.1002/pi.6567

1 Introduction

Green hydrogen via electrolysis results a main player in the energy transition and can help to decarbonize key sectors such as industry and transport. As an energy carrier, hydrogen can expand the use of renewable power, across a power-to-X, or electron to molecule strategy. Based in its high energy density, it can be competitive in certain applications. Taking into account the possibility to be transported in pipelines, it becomes an attractive low-cost option as distributed fuel and energy storage option, providing flexibility to power generation systems [1]. As green hydrogen production devices, liquid alkaline water electrolysers (LAWEs) dominate the market as the most mature technology. However, research and development is crucial to reduce costs, improving their competitiveness [2] and, in this context, the search of efficient materials and components is required. Furthermore, alkaline electrolyzers with anion exchange membranes (AEM), which combine the high efficiency of devices based in membrane electrode assemblies with the advantages of alkaline technologies, mainly the use of non-precious electrocatalysts, are now developed in laboratory level. As advanced materials, AEMs have shown a growing interest in several fields [3, 4], both energy and environment related, such as fuel cell [5, 6], heavy metal removal [7] and desalination [8],

Fixed-charge AEMs containing cationic groups (CGs) bounded to a polymer backbone were reported by several authors. Quaternary ammonium (QA) groups as fixed charges can be prepared by reaction of chloromethyl groups with tri-methylamine, being chloromethyl groups introduced by grafting of poly(vinylbenzyl chloride) (PVBC) onto a fluorinated ethylene propylene copolymer [9] or by chloromethylation of polysulfone [10].

A desirable property in AEMs is its chemical stability in operational conditions [11]. To avoid the low chemical stability of QA head groups by hydroxide anions attack from affecting the performance and stability of AEMs [12–14], other head groups were proposed, such as imidazolium groups [15, 16] and aliphatic amines, mostly 1,4-diazabicyclo[2.2.2]octane (DABCO) [17, 18]. Geometric restrictions from N-cyclic QA groups makes the hydroxide anion attack unfavorable, turning them stable in alkaline medium [14].

Lu *et al.* [19] reported an AEM based in polybenzimidazole (PBI) with PVBC, with DABCO as quaternizing agent, denoted PBI-c-PVBC/OH, that showed good performance in alkaline hydrogen fuel cell testing. Hao *et al.* [20] improved the performance of this membrane by

replacing DABCO by 1-butyl-1,4-diazabicyclo[2.2.2]octan-1-ium bromide (BDABCO) increasing the charge density of the membrane.

Recently, we reported membranes based in poly(2,5-benzimidazole) (ABPBI) crosslinked with PVBC with DABCO as quaternizing agent, applied to zero gap LAWEs [21]. The best results in terms of ionic conductivity and LAWE performance were attained with ABPBI/PVBC 1:2 molar ratio, and quaternized by immersion in a 0.5 mol·L-1 ethanolic solution of DABCO. Based in this results, we decided to study the effect of replacing DABCO by two DABCO alkyl derivatives in our previously reported membranes. In this kind of membranes, apart from the role of CGs and their OH^- counter ions, polybenzimidazole, as an anion solvating polymer matrix in association with an alkaline hydroxide solution, also contributes to the anionic conductivity. Therefore, the purpose of this research was twofold: to synthesize 1-butyl-1,4-diazabicyclo[2.2.2]octan-1-ium bromide (BDABCO) and 1-tetradecanyl-1,4-diazabicyclo[2.2.2]octan-1-ium bromide (TDABCO) as CG for AEMs, and tested its performance. The effect of an additional charge in the CG and the length of the carbon chain was evaluated.

2 Experimental

2.1 Materials

The ABPBI polymer, averaged molecular weight was 23,200 $g \cdot mol^{-1}$, was obtained by condensation of 3,4-diaminobenzoic acid (DABA, 97 wt. %, Aldrich) in polyphosphoric acid (PPA, 85 wt. %, Aldrich) according to a reported procedure [22]. Poly(vinylbenzyl chloride) (PVBC, 60/40 mixture of 3- and 4-isomers with average molecular weight M_w ~55,000 and M_w ~100,000 respectively, Sigma Aldrich), 1, 4-diazabicyclo[2.2.2]octane (DABCO, 99 wt. %, Sigma Aldrich), lithium nitrate ($LiNO_3$, 95 wt. %, Sigma Aldrich), potassium hydroxide (KOH, 85 wt. %, Sigma Aldrich), *N*-methyl-2-pyrrolidone (NMP, 99.8 wt. %, Carlo Erba), ethanol (absolute, Merck), 1-bromobutane (C_4H_9Br) (p.a., Merck), 1-bromotetradecane ($CH_3(CH_2)_{12}CH_2Br$, (97 % wt. %, Sigma-Aldrich) and ethyl acetate (EtOAc) (p.a., Merck) were used as received without further purification.

2.2 Alkyl substitution of DABCO

BDABCO and TDABCO were synthesized from alkyl substitution of DABCO, as is schematized in Fig. 1.

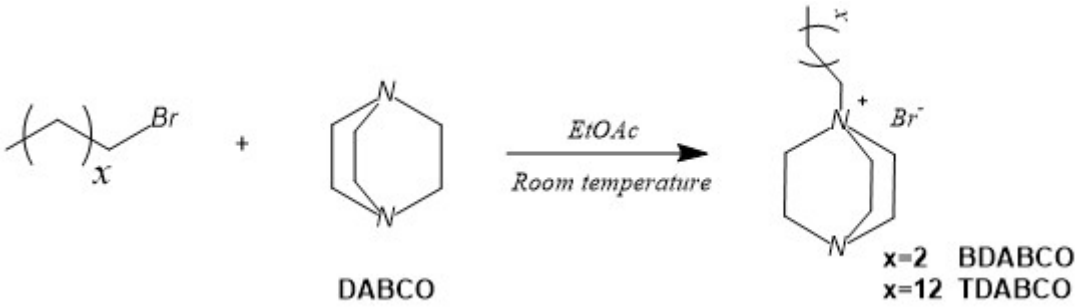

Fig. 1. Preparation pathway of BDABCO and TDABCO

BDABCO was prepared by mixing 10 wt. % DABCO in EtOAc with 1-bromobutane (molar ratio C_4H_9Br: DABCO 1:2), at room temperature, during 16 h. The obtained product was filtered, thoroughly washed with EtOAc, and vacuum dried, at 60 ºC for 24 h.

BDABCO: ^{1}H NMR (200 MHz, $CDCl_3$, 298 K): δ (ppm) 0.77 (3H, t, CH_2-C<u>H</u>$_3$), 1.20 (2H, m, CH_2-C<u>H</u>$_2$-CH_3), 1.57 (2H, m, CH_2-C<u>H</u>$_2$-CH_2), 3.05 (6H, t, N-C<u>H</u>$_2$-CH_2), 3.26 (2H, t, N^+-C<u>H</u>$_2$-CH_2), 3.45 (6H, t, N^+-C<u>H</u>$_2$-CH_2). ^{13}C NMR (200 MHz, $CDCl_3$, 298 K): δ (ppm) 13.55 (C, CH_2-<u>C</u>H$_3$), 19.58 (C, CH_2-<u>C</u>H$_2$-CH_3), 23.73 (C, CH_2-<u>C</u>H$_2$-CH_2), 45.21 (3C, N-<u>C</u>H$_2$-CH_2), 52.25 (3C, N^+-<u>C</u>H$_2$-CH_2), 64.18 (C, N^+-<u>C</u>H$_2$-CH_2).

TDABCO was prepared by mixing 10 wt. % of DABCO in EtOAc with 1-bromotetradecane (molar ratio $CH_3(CH_2)_{12}CH_2Br$: DABCO 1:2), at room temperature, during 16 h. The obtained product was filtered, thoroughly washed with EtOAc, and finally vacuum dried, at 60 ºC, for 24 h.

TDABCO: ^{1}H NMR (200 MHz, $CDCl_3$, 298 K): δ 0.81(ppm) (3H, t, CH_2-C<u>H</u>$_3$), 1.25 (22H, m, CH_2-C<u>H</u>$_2$-CH_2), 1.71 (2H, m, CH_2-C<u>H</u>$_2$-CH_2), 3.21 (6H, t, N-C<u>H</u>$_2$-CH_2), 3.41 (2H, m, N^+-C<u>H</u>$_2$-$CH_2(CH_2)_{12}CH_3$), 3.61 (6H, N^+-C<u>H</u>$_2$-CH_2). ^{13}C NMR (200 MHz, $CDCl_3$, 298 K): δ (ppm) 14.06 (C, CH_2-<u>C</u>H$_3$), 22.10 (C, CH_2-<u>C</u>H$_2$-CH_2), 22.61, 26.38, 29.17, 29.28, 29.37, 29.41, 29.54, 29.57, 29.61, 31.84 (11C, CH_2-<u>C</u>H$_2$-CH_2), 45.39 (3C, N-<u>C</u>H$_2$-CH_2), 52.44 (3C, N^+-<u>C</u>H$_2$-CH_2), 64.57 (C, N^+-<u>C</u>H$_2$-CH_2).

2.3 Preparation of ABPBI-c-PVBC/OH membranes

The crosslinked ABPBI-c-PVBC membranes were produced following a previously reported procedure by Coppola *et al.* [21]. The membranes, with molar ratio ABPBI: PVBC 1:2, were prepared by the casting method, from a solution of ABPBI (1 wt. %), $LiNO_3$ (1 wt. %) and

PVBC in NMP. The mixture was placed in a Petri dish and dried in an oven at 100 ºC for 48 h.

The quaternization of the ABPBI-c-PVBC films was made by immersion in a 0.5 $mol \cdot L^{-1}$ ethanolic solution of the quaternizing agent (BDABCO or TDABCO), at 60 ºC, for 24 h. Obtained membranes were denoted as ABPBI-c-PVBC/CG/Cl where CG is either BDABCO or TDABCO. Finally, the films were immersed in a 1 $mol \cdot L^{-1}$ KOH aqueous solution for 48 h getting the ABPBI-c-PVBC/CG/OH membranes. This preparation pathway is schematized in Fig. 2.

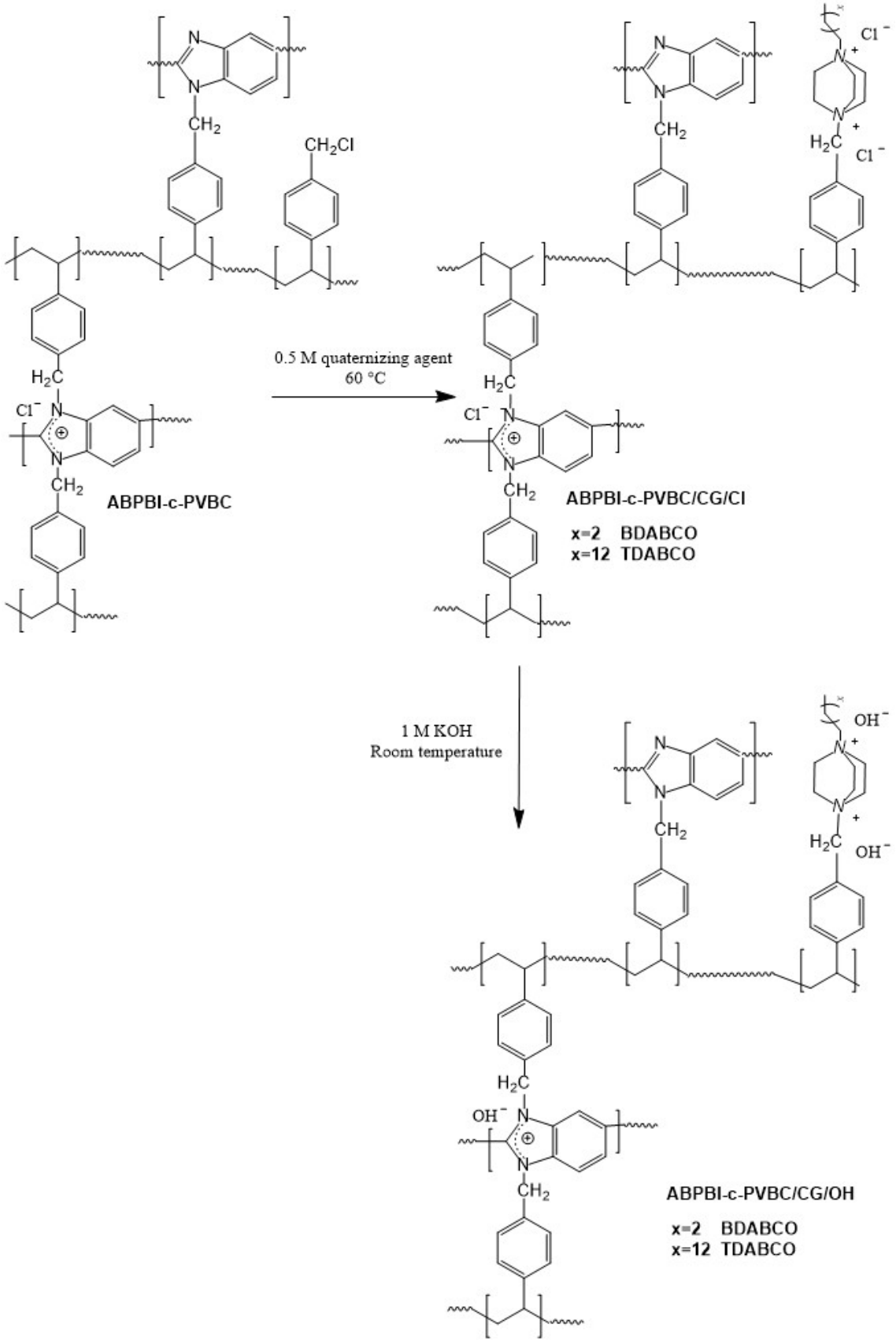

Fig. 2. Preparation pathway of ABPBI-c-PVBC/CG/OH membranes, where CG is either BDABCO or TDABCO.

The quaternization of the ABPBI-c-PVBC films with DABCO was prepared by immersion in a 0.5 mol·L^{-1} ethanolic solution of DABCO and then immersed the membrane in a 1 mol·L^{-1} KOH solution, according to the previously described procedure [21]. The membrane obtained was denoted as ABPBI-c-PVBC/DABCO/OH.

The membrane samples were maintained immersed in a 1 mol·L^{-1} KOH solution in N_2 atmosphere until measurements, in order to avoid the conversion of OH ion forms to bicarbonate ion forms by effect of carbon dioxide presence in the air.

2.4 Characterization of materials and membranes

2.4.1 Structure, surface morphology, chemical composition and stability in alkaline environment

The structure of the purified CG was verified by proton (^{1}H) and carbon (^{13}C) nuclear magnetic resonance (NMR) spectroscopies using a Bruker AC 200, employing deuterium chloroform as solvent. Fourier transform infrared spectroscopy (FTIR) measurements were made with a Thermo Scientific Nicolet 6700 FTIR spectrometer. Scanning electron microscopy (SEM) was employed to analyze the surface morphology and chemical composition, carried out in a Philips 505, equipped with an energy dispersive x-ray spectroscopy device (EDS) operated at 20 kV (1 μm penetration depth). The membrane stability was evaluated in an alkaline environment. The membrane samples were immersed for 20 days in a 1 mol·L-1 KOH solution at 70 °C.

2.4.2 Thermal properties and water contact angle

Thermogravimetric analysis (TGA) was employed to measure the thermal properties of the membranes by means of a Netzsch STA 449C instrument. For this purpose, samples of 10-30 mg were placed in an aluminum crucible and then heated from 30 °C to 550 °C at a rate of 10 °C/min, under an argon atmosphere. Water contact angle was determined as the averaged contact angle of ten different measurements, each one consisting in ten images taken during ten seconds. Image analysis was carried out using the ImageJ software.

2.4.3 Swelling ratio, KOH and water uptake

The swelling ratio (SR) was determined by measuring the thickness, width and length with a Mitutoyo AOS Digimatic Caliper before and after immersing a previously dried membrane in 1 mol·L^{-1} KOH solution at room temperature during 1 h.

For KOH and water uptake measurements, ABPBI-c-PVBC/CG/Cl membrane samples were first immersed in 1 mol·L^{-1} KOH solution for 1 h, changing it by fresh solution every 20 min. Then, they were washed several times with distillate water until neutral pH was attained in order to eliminate the free KOH and then dried in vacuum oven at 40 ºC until constant weight (w_0). w_0 is considered the dry weight of membrane samples in OH^- form. Next, the samples were immersed in 1 mol·L^{-1} KOH aqueous solution during 48 h, then removed and weighed after being dried carefully with tissue paper (w_s). w_s is considered the wet weight. At last, the samples remained overnight at 40 ºC under vacuum, and weighed until constant weight (w_d). The polymer content, water and KOH uptake were determined with the equations:

$$Polymer\ (\%) = \frac{w_0}{w_s} \times 100 \quad (1)$$

$$KOH\ uptake\ (\%) = \frac{(w_d - w_0)}{w_0} \times 100 \quad (2)$$

$$H_2O\ uptake\ (\%) = \frac{(w_s - w_d)}{w_0} \times 100 \quad (3)$$

2.4.4 Ionic exchange capacity measurement

The ion exchange capacity (IEC) of the ABPBI-c-PVBC/CG/OH membranes were determined potentiometric by acid-base titration. The membranes were immersed for 24 h in 50 mL of 1 mol·L^{-1} NaCl aqueous solution. The immersion solution with the membrane inside was titrated with a standardized 0.02 mol·L^{-1} H_2SO_4 solution. Analyses were performed on triplicate with a Metrohm Titrando 852. Finally, the membranes were thoroughly washed with distillate water and dried in a vacuum oven (40 ºC, 100 mbar) until constant weight ($w0$). IEC (mmol g^{-1}) was determined as:

$$\text{IEC} = \frac{Ep \cdot 0.02}{w0} \quad (4)$$

where E_p, is the equivalence point, in mL.

2.4.5 Ionic conductivity

The ionic conductivity was measured by Electrochemical Impedance Spectroscopy (EIS) in a temperature range between 25 ºC and 80 ºC, with an Autolab PGSTAT 30N coupled to a frequency response analyzer (FRA) and a two-point cell composed of two stainless steel plates

in contact with both sample faces, as it was previously described [23]. The membrane samples remained immersed in a 1 mol·L^{-1} KOH aqueous solution for no less than 48 h. Then they were removed from the solution, surface dried with a tissue paper and placed in the cell. The specific ionic conductivity, σ (S·cm^{-1}), was determined by the equation:

$$\sigma = \frac{L}{RA} \tag{5}$$

where R is the ohmic resistance (Ω) resulting from the real axis intercept of the Nyquist plot, L (cm) is the thickness of the sample, and *A* (cm^2*)* is the active surface area (0.36 cm^2).

The activation energy was calculated with the Arrhenius equation:

$$\sigma = \sigma_0 \cdot exp - \left(\frac{E_a}{RT}\right) \tag{6}$$

Being σ the conductivity, σ_0 the maximum conductivity, R is the gas constant and E_a is the activation energy for the ionic conduction.

In order to avoid the conversion of hydroxyl ions to bicarbonate ion forms as a consequence of carbon dioxide present in the air, the membrane samples were introduced to the conductivity cell under wet conditions, and the conductivity measurement was performed immediately.

2.5 Alkaline water electrolysis

The performances of the membranes in a laboratory-scale water electrolyzer of zero gap configuration as reported elsewhere [21] were evaluated. The electrolyzer cell was composed by two nickel foam electrodes (Sigma Aldrich, thickness 1.6 mm, bulk density 0.45 g cm^{-3} and porosity 95%) of 3.61 cm^2 geometric area, directly in contact with both membrane faces, and two gold electroplated Ni sheets as current feeders and electrolyte distributors. A 1 mol·L^{-1} KOH aqueous solution was circulated by means of a Master Flex peristaltic pump. The current density-potential curves were measured in the 1.5-2.0 V range at 50 °C. In chronopotentiometric measurements, a current density of 200 mA·cm^{-2} was applied for 60 min, with a temperature of 50 °C.

3 Results and discussion

3.1 Structure Characterization

BDABCO and TDABCO were synthetized from alkyl substitution of DABCO, obtaining crystalline white solids, with molar yields of 92% and 97%, respectively. The connectivity of their carbon and hydrogen atoms was analyzed from $^{1}H - ^{13}C$ COSY 2D NMR spectroscopy.

Successful quaternization between chloromethyl groups from the ABPBI-c-PVBC membrane and the CG was analyzed by FTIR. Fig. 3 shows the FTIR spectra of ABPBI, PVBC, BDABCO, TDABCO and crosslinked ABPBI-c-PVBC membranes, before and after quaternization. A clear rise in the alkyl group band at 2800 cm^{-1} is observed due to the presence of alkyl chains form BDABCO and TDABCO in the quaternized membrane. The 1267 cm^{-1} signal, assigned to the stretching of the chloromethyl groups, is vanished for the ABPBI-c-PVBC/CG/OH due to the substitution of chlorine by CG, as a result of the quaternization reaction. This reaction is also evidenced from the small and sharp signal at 1060 cm^{-1} and 1460 cm^{-1} in the ABPBI-c-PVBC/CG/OH spectrum, which can be assigned to the stretching of the quaternary ammonium groups [19-21].

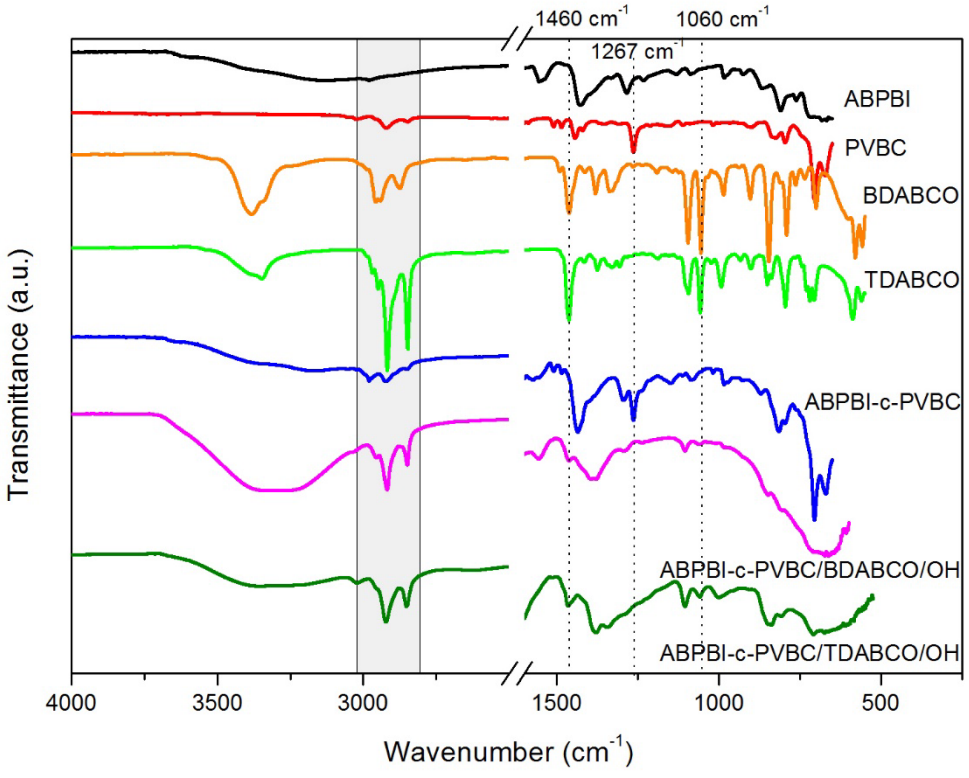

Fig. 3. FTIR spectra of ABPBI, PVBC, BDABCO, TDABCO and membranes.

The surface morphology and chemical composition of the membranes, before and after the quaternization stage with BDABCO and TDABCO were analyzed.

Fig. 4 shows the SEM images and EDS spectra of the membranes ABPBI-c-PVBC, ABPBI-c-PVBC/BDABCO/OH and ABPBI/TDABCO/OH.

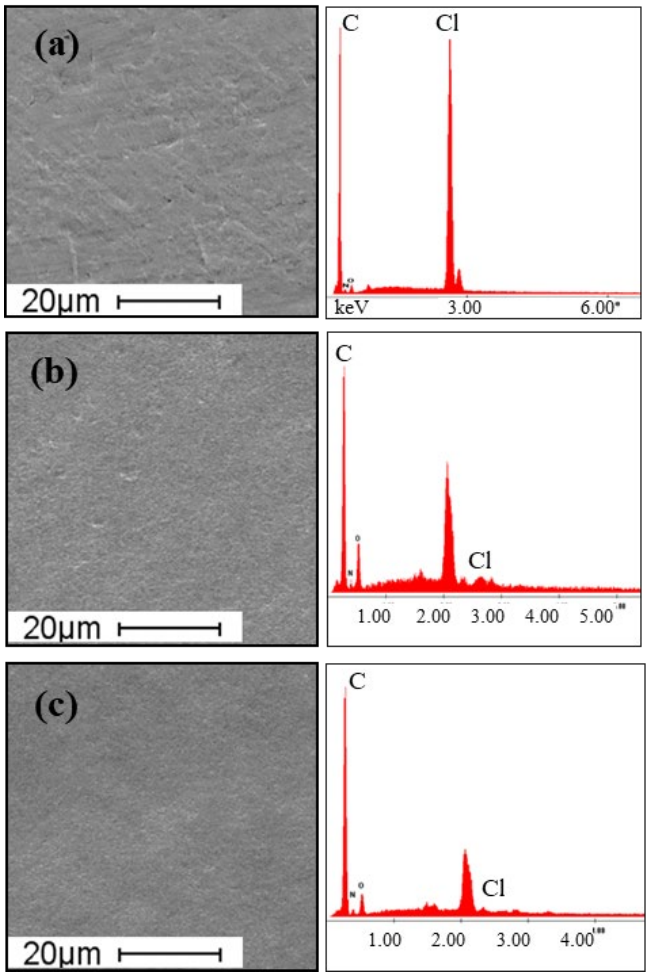

Fig. 4. SEM images and EDS spectra of the membranes a) ABPBI-c-PVBC, b) ABPBI-c-PVBC/BDABCO/OH and c) ABPBI/TDABCO/OH.

SEM images show that all the membranes have a homogeneous microstructure, without phase segregation. EDS spectra show a high pick corresponding to chlorine element, due to chloromethyl groups, in the membrane before quaternization stage (ABPBI-c-PVBC), which is reduced in the rest of the membranes, hence confirming quaternization by incorporation of BDABCO and TDABCO, respectively.

To evaluate the chemical stability of the ABPBI-c-PVBC/CG/OH membrane, they were immersed in a 1 mol·L^{-1} KOH solution at 70 °C. After 20 days, no visible changes in the properties (color and integrity) of the samples were observed.

Thermal stability of the membranes was studied by thermogravimetric analysis. Fig. 5 shows that all membranes are stable until around 150 °C, where a loss of water in the membranes is observed. At 350 °C, the degradation of the crosslinking point between a moiety -NH- of ABPBI and a CH_2Cl group takes place [21]. These results allows to conclude that thermal stability of the membranes is adequate for its use in low temperature alkaline water electrolyzers, which operate below 100 °C.

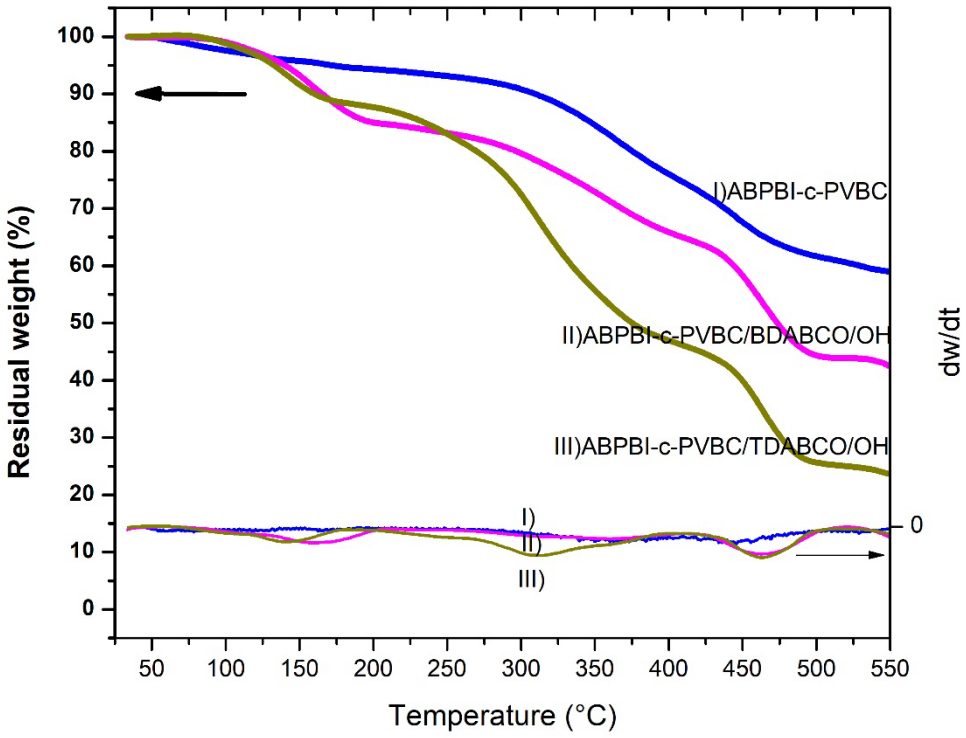

Fig. 5. TGA thermographs of ABPBI-c-PVBC and ABPBI-c-PVBC/CG/OH membranes.

The effect of the CG in the membrane surface structure was analyzed by measuring the water contact angle. Table 1 shows the water contact angle for ABPBI-c-PVBC/CG/OH. For comparison purposes, ABPBI-c-PVBC/DABCO/OH water contact angle is shown. An increase in water contact angle is observed for ABPBI-c-PVBC/TDABCO/OH, meaning the length of the aliphatic chain plays a key role in the surface hydrophobicity. This effect is also observed in the water and KOH uptake (Table 1).

Membrane	Water contact angle/ º	KOH/ wt. %	H_2O/ wt. %

ABPBI-c-PVBC/DABCO/OH	70 ± 2	11 ± 1 [21]	51 ± 7 [21]
ABPBI-c-PVBC/BDABCO/OH	72 ± 3	13 ± 2	55 ± 1
ABPBI-c-PVBC/TDABCO/OH	80 ± 3	7 ± 1	20 ± 2

Table 1. Water contact angle, KOH and H_2O uptake for ABPBI-c-PVBC/DABCO/OH, ABPBI-c-PVBC/BDABCO/OH and ABPBI/TDABCO/OH membranes.

3.2 Thickness increase and ion change capacity

Swelling results for membranes soaked 1 h in a 1 $mol \cdot L^{-1}$ KOH aqueous solution at room temperature are show in Table 2, along with IEC. For comparison purposes, swelling ratio and IEC of ABPBI-c-PVBC/DABCO/OH is also included [21].

Membranes SR is strongly related to the molecular interactions between solvent and polymer chains, among other effects. As can be seen, the ABPBI-c-PVBC/TDABCO/OH membrane has the lowest SR, owed to its low water sorption, related with its hydrophobic character. The same effect is observed in its IEC, meaning that the membrane has a lower exchangeable OH group density.

Based on the measured IEC, the ABPBI-c-PVBC/BDABCO/OH membrane possesses the highest density of cationic charges, owing to the quaternizing agent's doubly charged short alkyl chain with two QA groups. Previous studies generally indicated that the presence of flexible side chains induces phase separation, favoring the formation of well-hydrated and percolated conductive domains [24].

In the case of the ABPBI-c-PVBC/TDABCO/OH membrane, despite the quaternizing agent having a doubly charged alkyl chain, the obtained IEC was still lower than in the case of DABCO. Coupled with its low water and KOH content, we can infer that an optimal packing occurs with n = 4 carbon atoms in the alkyl chain, suggesting that longer alkyl chains would increase the AEM's hydrophobicity.

A future challenge lies in studying the conformation and aggregation of the side chains to elucidate the specific mechanisms underlying these effects. Further research in this direction will provide valuable insights into tailoring AEM properties for enhanced performance in various electrochemical applications.

Membrane	VSR/ %	TSR/ %	LSR/ %	IEC/ mmol·g^{-1}
ABPBI-c-PVBC/DABCO/OH [21]	90 ± 13	38 ± 3	21 ±7	1.70 ± 0.03
ABPBI-c-PVBC/ BDABCO/OH	48 ± 5	27 ± 4	8 ± 2	2.13 ± 0.02
ABPBI-c-PVBC/TDABCO/OH	12 ± 4	6 ± 4	3 ± 1	0.82 ± 0.04

Table 2. Swelling behavior: SR (swelling ratio), VSR (volume SR), TSR (thickness SR), LSR (length SR), IEC (ion exchange capacity) for ABPBI-c-PVBC/DABCO/OH, ABPBI-c-PVBC/BDABCO/OH and ABPBI/TDABCO/OH membranes.

3.3 Conductivity

In Fig. 6 is shown the anionic specific conductivity of ABPBI-c-PVBC/CG/OH membranes. The highest conductivity was obtained for ABPBI-c-PVBC/BDABCO/OH, with a value of (0.080 ± 0.005) S·cm^{-1} at 80 °C. The activation energy for the ionic conduction (Ea) derived from equation (6), falls between 4.3 kJ·mol^{-1} for ABPBI-c-PVBC/BDABCO/OH and 6.4 kJ·mol^{-1} for ABPBI-c-PVBC/TDABCO/OH, a common range for this kind of membranes [21].

The anionic specific conductivity of ABPBI-c-PVBC/CG/OH membranes follows the tendency of water and KOH sorption and IEC results. These parameters are related, since the CG affects the structure of the membrane and therefore its ion transport properties. Additionally, as it was pointed out earlier, the anionic conduction of this kind of membrane is related not only to the presence of CGs, but also to the captured KOH linked to the polybenzimidazole molecules, acting as ion solvating polymer. Captured KOH provide OH^- counter ions linked to the CG groups and, on the other hand, undergo acid-base reactions with acid sites in ABPBI molecule, forming potassium polybenzimidazolate salt and water. Once each CG group have its corresponding OH^- counter ion, and once all acid sites in ABPBI polymer are in the potassium form, additional potassium hydroxide remains as free KOH inside the membrane. Linked and free OH^- contribute to the ion conducting mechanism, that combines diffusion, migration, convection and Grotthuss, which is considered to play the most important role, based on hydroxide transport through the membrane by the formation and cleavage of hydrogen bonds with the surrounding water molecules [21].

Considering the poor performance of ABPBI-c-PVBC/TDABCO/OH membrane, according to IEC and conductivity results, this membrane was not taken in account in alkaline water electrolyzer measurements.

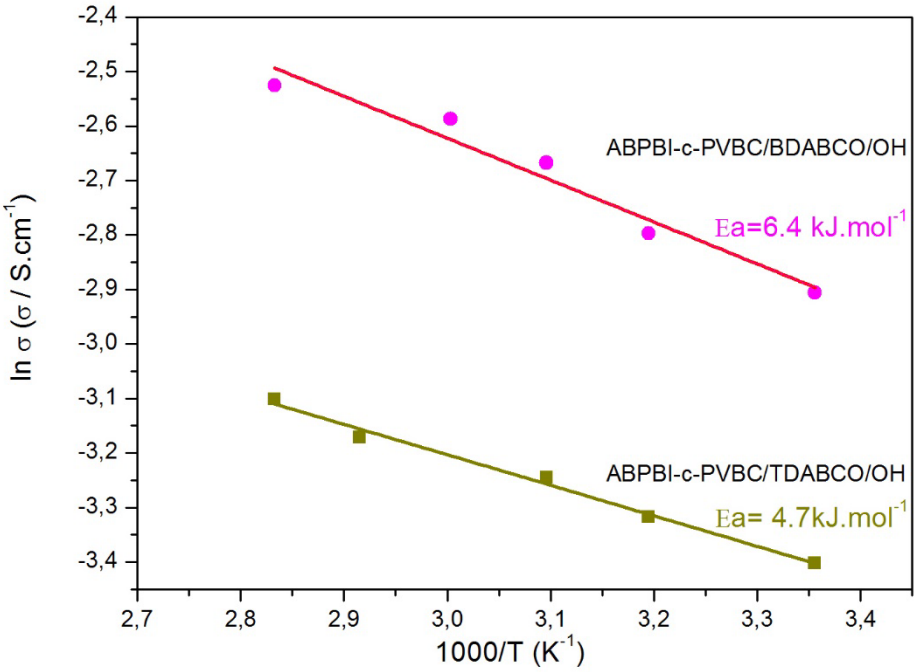

Fig. 6. Arrhenius plots for ABPBI-c-PVBC/GC/OH membranes

3.4 Alkaline water electrolysis

Fig. 7 shows both polarization curves and chronopotentiometric measurements in a 1 mol·L^{-1} KOH solution at 50 °C and 70 °C for ABPBI-c-PVBC/BDABCO/OH. Chronopotentiometric measurements were performed with a current density of 200 mA·cm^{-2}. At 1.98 V, the membrane has a current density of 438 mA·cm^{-2} and 497 mA·cm^{-2} at 50°C and 70°C, respectively.

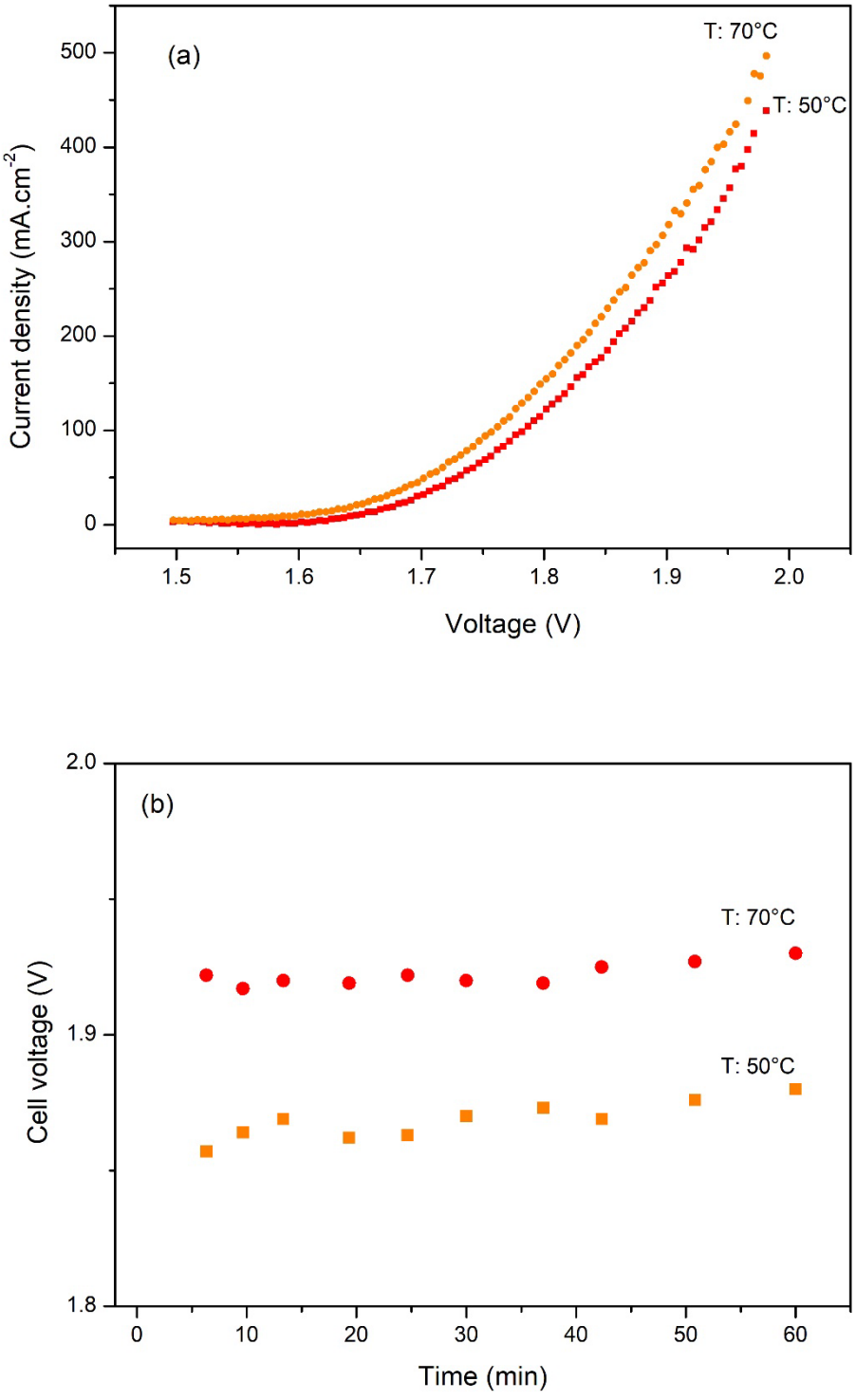

Fig. 7. Performance of ABPBI-c-PVBC/BDABCO/OH membranes in 1M KOH at 50 ºC and 70 ºC, a) polarization curves at and b) chronopotentiometric curve at i = 200 mA·cm^2.

Table 3 compares the performance of previously reported membranes used in zero gap LAWEs. As can be seen, the performance attained in this work is superior than that of our

previous work in same conditions with other membranes [21, 22] and that of alkaline electrolyzers with Ni electrodes and high KOH concentration [25-27]. These last membranes with a greater thickness. The mild operative conditions of the electrolyzer, such as low KOH concentration and temperature, and the use of a commercially available electrode material such as Nickel foam, makes this findings promising.

However, much more outstanding results in terms of efficiency and performance can be achieved by jointly addressing not only the optimization of the membrane but also the catalyst. This is clearly demonstrated in the work carried out by Li Wang and co-workers, who used the 2,2″,4,4″,6,6″-hexamethyl-p-terphenylene-polydimethylbenzimidazolium (HTM-PMBI) membrane and compared the performance of an electrolyzer using different catalysts. They found that the best results were obtained when using NiAlMo electrodes, sprayed onto a dense film of stainless steel gradient porous metal framework (GPMF, MeliCon GmbH) [28]. On the other hand, a high-performance Anion Exchange Membrane (AEM) electrolyzer equipped with a $Ni(OH)_2$-Fe anode was reported, using the Tokuyama A201 membrane [29].

Therefore, carrying out future work to improve their properties and performance in zero gap LAWE is the next step to make them commercially attractive. In our future work, we propose to optimize the design of our electrolyzer using the promising membrane that we have reported in this study.

Electrolyzer	**Membrane (thickness)**	**Electrode materials**	**T / ºC**	**Circulation of KOH / mol · L^{-1}**	**Cell voltage / V**	**Current density / mA·cm^{-2}**
This work	ABPBI-c-PVBC/BDABCO/OH (60 µm)	Ni foam	50	1	1.98	438
		Ni foam	70	1	1.98	497
[21]	ABPBI-c-PVBC/DABCO/OH (60 µm)	Ni foam	50	1	1.98	380
[21]	PBI-c-PVBC/DABCO/OH (60 µm)	Ni foam	50	1	1.98	380
[22]	Zirfon® (300 µm)	Ni foam	50	3	2.0	140
Hydrogenics [25,26]	Porous diaphragm (PD) (300 µm)	Ni sheet	80-90	6.7	1.7	375
Teletype [25,26]	PD (300 µm)	Ni sheet	80-90	6.7	2.2	300

Uralkhimmash [25,26]	PD (300 μm)	Ni sheet	80-90	6.7	2.3	200
[27]	Fumatech FAA-3-50 (50 μm)	Ni foam	60	2.3	2	30
[28]*	Hexamethyl-p-terphenyl poly-(benzimidazolium) (HMT-PMBI) (50 μm)	NiAlMo / Plasma spray/ GPMF	60	1	2.0	1900
[29]**	Tokuyama A201 (28 μm)	Anode: Ni(OH)2-Fe /Cathode: Raney NiMo	50	1	2.05	2000

*Optimized electrodes of NiAlMo, sprayed on dense film of stainless steel gradient porous metal framework (GPMF, MeliCon GmbH).

**In both catalytic layers multi-walled carbon nanotubes (CNT, BAYTUBES C 70 P, Bayer MaterialScience AG) were added as additives and Sustainion XA-9 Alkaline Ionomer was used as ionomer.

Table 3. Performance of zero gap LAWE cell for commercially available AEMs and polibenzimidazole-c-PVBC-based membranes.

4. Conclusions

BDABCO and TDABCO were synthesized with yields higher than 90%, without secondary products or impurities, as demonstrated by ^{1}H NMR measurements. The quaternization of ABPBI-c-PVBC membranes with BDABCO and TDABCO was successfully done, as demonstrated by FTIR spectra and EDS spectra. The incorporation of an extra CG improved IEC, conductivity and electrolyzer performance. AEMs quaternized with TDABCO showed lower IEC and conductivity than that of AEMs quaternized with BDABCO, possible caused by the excessive length of the carbon chain, decreasing the CG density. The simple pathway of DABCO alkylation allows to modify the CG properties and therefore the membrane performance. Further studies regarding the durability of the reported membranes under LAWE conditions are required.

Acknowledgments

The authors would like to acknowledge INTI and CONICET for the support provided.

Conflict of interest

The authors declare no conflict of interest.

References

[1] IRENA, *Reaching zero with renewables: Eliminating CO2 emissions from industry and transport in line with the 1.5oC climate goal*, International Renewable Energy Agency, Abu Dhabi, 2020. ISBN 978 - 92 - 9260 - 269 - 7. Available for download: www.irena.org/publications

[2] IEA, *Hydrogen*, IEA, Paris, 2020, https://www.iea.org/reports/hydrogen.

[3] Chen Z, Huang D, Hwang JY, *Polym. Int.*, **68.5:** 972-978 (2019).

[4] Flachard D, Serghei A, Fumagalli M, Drockenmuller E, *Polym. Int.*, ***68.9***: 1591-1598 (2019).

[5] Henkensmeier D, et al., *J. Electrochem. Energy Convers* **18.2** (2021).

[6] Albayrak Arı G, Şimşek Ö, *Polym. Int.*, ***69.7:*** 644-652(2020).

[7] Coppola RE, Lozano HE, Contin M, Canneva A, Molinari FN, Abuin GC, D'Accorso NB, *Polym. Int.*, ***71.9:*** 1143-1151 (2022).

[8] Sharma J, Mishra S, Rathod NH, Kulshrestha V, *J. Memb. Sci.*, ***66:*** 121082 (2022).

[9] Slade RCT, Varcoe JR, *Solid State Ionics*. **176:** 585–597 (2005).

[10] Abuin GC, Franceschini EA, Nonjola P, Mathe MK, Modibedi M, Corti HR, *J. Power Sources.* **279:** 450–459 (2015).

[11] Tuli SK, Roy AL, Elgammal RA, Zawodzinski TA, Fujiwara T, *Polym. Int.*, **67.9:** 1302-1312 (2018).

[12] Klaus-Dieter Kreuer, Fossil Energy: Selected Entries from the Encyclopedia of Sustainability Science and Technology, 2013. doi:10.1007/SpringerReference_29671.

[13] Espiritu R, Golding BT, Scott K, Mamlouk M, *J. Mater. Chem. A.* **5**: 1248–1267 (2017).

[14] Chu X, Liu L, Huang Y, Guiver MD, Li N, *J. Memb. Sci.* **578:** 239–250 (2019).

[15] Gao X, Lu F, Liu Y, Sun N, Zheng L, *Chem. Commun.* **53**: 767–770 (2017).

[16] Lu W, Shao ZG, Zhang G, Zhao Y, Yi B, *J. Power Sources.* **248:** 905–914 (2014).

[17] Zhang K, Drummey KJ, Moon NG, Chiang WD, Long TE, *Polym. Chem.* **7:** 3370–3374 (2016).

[18] Hnát J, Plevová M, Žitka J, Paidar M, Bouzek K, *Electrochim. Acta.* **248:** 547–555 (2017).

[19] Lu W, Zhang G, Li J, Hao J, Wei F, Li W, Zhang J, Shao ZG, Yi B, *J. Power Sources.* **296:** 204–214 (2015).

[20] Hao J, Jiang Y, Gao X, Lu W, Xiao Y, Shao Z, Yi B, *J. Memb. Sci.* **548:** 1–10 (2018).

[21] Coppola RE, Herranz D, Escudero-Cid R, Ming N, D'Accorso NB, Ocón P, Abuin GC, *Renewable Energy* **157:** 71-82. (2020).

[22] Diaz LA, Hnát J, Heredia N, Bruno MM, Viva FA, Paidar M, Corti HR, Bouzek K, Abuin GC, *J. Power Sources.* **312:** 128–136 (2016).

[23] Diaz LA, Coppola RE, Abuin GC, Escudero-Cid R, Herranz D, Ocón P, *J. Memb. Sci* **535:** 45 - 55 (2017).

[24] Jannasch, P., & Weiber, E. A., *Macromol Chem Phys*, **217.10**: 1108-1118 (2016).

[25] Jensen JO, Bandur V, Bjerrum NJ, Jensen SH, Ebbesen SD, Mogensen M, Tophøj N, Yde L, Pre-investigation of water electrolysis, PSO-F&U 2006-1-6287, project 6287 PSO, 1–195 (2006).

[26] Bertuccioli L, Chan A, Hart D, Lehner F, Madden B, Standen E, Study on development of water electrolysis in the EU - Final Report, *Fuel Cells Hydrog. Jt. Undert.* (2014).

[27] Lee N, Duong DT, Kim D, *Electrochim. Acta*, **271:** 150–157 (2018).

[28] Wang L, *et al.*, *ACS Applied Energy Materials* **2.11:** 7903-7912 (2019).

[29] Wang L, *et al.*, *ACS Applied Energy Materials* **5.2:** 2221-2230 (2022).

Synthesis, characterization and performance of new DABCO derivatives in anion exchange membranes

R.E. Coppola, N.B. D'Accorso, G.C. Abuin

Two double-charge anion exchange membranes based on polybenzimidazole and poly(vinylbenzyl chloride) were prepared, characterized and evaluated for its use in a zero-gap water alkaline electrolyzer.